J Elast (2012) 106:123–147
DOI 10.1007/s10659-011-9313-x

Instabilities of Hyperelastic Fiber Composites: Micromechanical Versus Numerical Analyses

Stephan Rudykh · Gal deBotton

Received: 28 February 2010 / Published online: 2 February 2011

Abstract Macroscopic instabilities of fiber reinforced composites undergoing large deformations are studied. Analytical predictions for the onset of instability are determined by application of a new variational estimate for the behavior of hyperelastic composites. The resulting, closed-form expressions, are compared with corresponding predictions of finite element simulations. The simulations are performed with 3-D models of periodic composites with hexagonal unit cell subjected to compression along the fibers as well as to non-aligned compression. Throughout, the analytical predictions for the failures of neo-Hookean and Gent composites are in agreement with the numerical simulations. It is found that the critical stretch ratio for Gent composites is close to the one determined for neo-Hookean composites with similar volume fractions and contrasts between the phases properties. During non-aligned compression the fibers rotate and hence, for some loading directions, the compression along the fibers never reaches the level at which loss of stability may occur.

Keywords Finite deformation · Instability · Bifurcation · Homogenization · Variational estimate · Fiber composite

Mathematics Subject Classification (2000) 74G60 · 74Q15

1 Introduction

Composite materials are widely used in various engineering areas. Therefore characterization of their properties is of importance for both engineering applications and theoretical development of methods that can reduce the need for high-cost experiments. An important

S. Rudykh · G. deBotton (✉)
The Pearlstone Center for Aeronautical Studies, Department of Mechanical Engineering, Ben-Gurion University, Beer-Sheva 84105, Israel
e-mail: debotton@bgumail.bgu.ac.il

G. deBotton
Department of Biomedical Engineering, Ben-Gurion University, Beer-Sheva 84105, Israel

and hard to predict characteristic is the one associated with loss of stability, also referred to as "local buckling". This phenomenon is mostly considered as a failure mode that should be predicted and avoided. However, in some cases, such as in "snap-through" mechanisms this phenomena can be used for our benefit (e.g., O'Halloran et al. [34]).

A fundamental study of this topic was performed by Biot [5], who developed a theory for pre-stressed rubber-like solids in finite deformation. Rosen [38] estimated the compressive strength of fiber composites based on beam theory. A general discussion concerning the bifurcation phenomena was provided by Hill and Hutchinson [19]. Among the methods that take into account imperfections in fiber composites we mention the works of Budiansky [6], Fleck [14] and Merodio and Pence [27]. The problem of a localized failure at the free surface of orthotropic materials was examined by deBotton and Schulgasser [9].

In composite materials bifurcations may occur at a scale which is significantly smaller than the size of the specimen. Triantafyllidis and Maker [40] determined the onset of instabilities in periodic layered media at such *microscopic* levels, as well as at *macroscopic* level. They noted that macroscopic instabilities that occur at a scale significantly larger than the scale of the microstructure can be detected with the help of the homogenized tensor of elastic moduli. Instabilities at smaller scales demanded usage of more complicated techniques such as Bloch wave analysis (e.g., Kittel [22]). Subsequently, Geymonat et al. [16] generalized this work and showed that Floqet theorem or Bloch wave technique can be applied for analyzing the characteristic unit cell and predicting the onset of failures at all scales.

Nestorovic and Triantafyllidis [30] determined loss of stability in 2-D layered composites subjected to combined shear and compression. Periodic fiber composites subjected to in-plane *transverse* deformation were numerically examined by Triantafyllidis et al. [41] for the case of neo-Hookean phases, and by Bertoldi and Boyce [4] for both neo-Hookean and Gent phases. Michel et al. [28] compared numerical results for the transverse behavior and loss of stability of periodic porous fiber composites with corresponding predictions of the variational estimate of Lopez-Pamies and Ponte Castañeda [24]. The 2-D finite element (FE) analyses performed in the above mentioned works did not cover instabilities due to compression *along* the fibers. This problem was considered *analytically* by Agoras et al. [2], who examined the responses of the composites under general loading conditions by application of the variational estimate of Agoras et al. [1], and the TIH model for fiber composites with neo-Hookean phases that was introduced in [12].

Loss of stability due to compression along the fibers is an important mode of failure (e.g., Merodio and Ogden [26], Qiu and Pence [37]). Therefore, in this work we make use of both analytical and numerical approaches to analyze the onset of this failure mode. The numerical analysis requires examination of 3-D models subjected to finite-strain loading conditions. Accordingly, in contrast to the FE models used in previous works, we develop a 3-D model and extend appropriate techniques for determining the onset of instabilities. Complementary to the numerical study, we determine analytical predictions for the onset of stability loss by application of the variational method of deBotton and Shmuel [11]. We will examine the effective response and stability loss of the neo-Hookean composites of deBotton et al. [12], and corresponding fiber composites with Gent phases. Additionally, a new upper estimate for composites with Gent phases is introduced. We emphasize that the analytical procedure results in *closed-form* estimates for the onset of failure.

Before we proceed we remark that in the preceding paragraphs a few variational estimates for characterizing the effective behaviors of hyperelastic composites were mentioned. In connection with those we recall that Ponte Castañeda [35] introduced a variational method for determining the effective properties of composites with mechanically nonlinear phases in the limit of infinitesimal elasticity. The usage of *linear comparison composites* whose overall behaviors are known and from which corresponding estimates for the behaviors of the

nonlinear composites can be extracted was the primary merit of this work. This concept was further extended to the class of geometrically nonlinear composites where linear comparison composites were used to obtain estimates for hyperelastic composites (e.g., Ponte Castañeda and Tiberio [36], Lopez-Pamies and Ponte Castañeda [25], Agoras et al. [1, 2] and references therein). More recently, deBotton and Shmuel [11] introduced a different variational method for the class of hyperelastic composites. In the spirit of the pioneering work of Ponte Castañeda [35] this method also makes use of comparison composites, however, the usage of *nonlinear comparison composites* instead of linear comparison composites is the merit of this new approach. For consistence, in accordance with the comparison media used in the different homogenization methods, we refer to the method followed by Agoras et al. [2] as the *linear comparison* (LC) variational estimate, and to the one developed by deBotton and Shmuel [11] as the *nonlinear comparison* (NLC) variational estimate. We conclude this remark noting that in some cases the predictions of the two methods may be quite close, but in general they are distinct (e.g., deBotton and Shmuel [11]). In the context of the present work, we will subsequently discuss the advantage of using hyperelastic comparison composites for estimating the critical stretch ratios at the onset of stability loss.

The work is structured as follows. A brief summary of the theory of finite elasticity including a discussion about the strong ellipticity condition is outlined in the theoretical background section. In Sect. 3 we recall the main results of the NLC estimate of deBotton and Shmuel [11] in the context of fiber composites, and determine the corresponding expression for the effective tensor of instantaneous moduli stemming from this estimate. The analytical expressions are specialized next to plane-strain loading conditions with the fibers lying in the plane of deformation. The hexagonal unit cell and the procedure developed for the numerical analysis are described in Sect. 4. Analytical and numerical estimates for the macroscopic stable domains of fiber composites with neo-Hookean and Gent phases under plane-strain conditions are presented in Sect. 5. A short summary concludes the work.

2 Theoretical Background

The Cartesian position vector of a material point in a reference configuration of a body $\mathcal{B}_0$ is $\mathbf{X}$, and its position vector in the deformed configuration $\mathcal{B}$ is $\mathbf{x}$. The deformation of the body is characterized by the mapping

$$\mathbf{x} = \boldsymbol{\chi}(\mathbf{X}). \tag{1}$$

The deformation gradient is

$$\mathbf{F} = \frac{\partial \boldsymbol{\chi}(\mathbf{X})}{\partial \mathbf{X}}. \tag{2}$$

We assume that the deformation is invertible and hence $\mathbf{F}$ is non-singular, accordingly

$$J \equiv \det \mathbf{F} \neq 0. \tag{3}$$

Physically, J is the volume ratio between the volumes of an element in the deformed and the reference configurations, and hence $J = \frac{dv}{dV} > 0$. For a *Green elastic* or *hyperelastic* material, the constitutive relation is given in terms of a scalar-valued strain energy-density function $\Psi(\mathbf{F})$ such that

$$\mathbf{P} = \frac{\partial \Psi(\mathbf{F})}{\partial \mathbf{F}}, \tag{4}$$

where $\mathbf{P}$ is the 1st Piola-Kirchhoff (nominal) stress tensor. The corresponding true or Cauchy stress tensor is related to the 1st Piola-Kirchhoff stress tensor via the relation

$$\boldsymbol{\sigma} = J^{-1}\mathbf{P}\mathbf{F}^T. \tag{5}$$

In the absence of body forces the equilibrium equation is

$$\nabla \cdot \boldsymbol{\sigma} = 0. \tag{6}$$

The strain energy-density function Ψ of an isotropic material can be expressed in terms of the three invariants of the Cauchy-Green strain tensor $\mathbf{C} \equiv \mathbf{F}^T\mathbf{F}$. It is common to express these invariants in the form

$$I_1 = \mathrm{Tr}\mathbf{C}, \qquad I_2 = \frac{1}{2}(I_1^2 - \mathrm{Tr}(\mathbf{C}^2)), \qquad I_3 = \det\mathbf{C}. \tag{7}$$

A widely used isotropic and incompressible model that enables to capture the "lock-up" effect of the molecular chain extension limit is the Gent [15] model (e.g., Horgan and Saccomandi [20])

$$\Psi_G = -\frac{1}{2}\mu J_m \ln\left(1 - \frac{I_1 - 3}{J_m}\right). \tag{8}$$

Here μ is the initial shear modulus and J_m is a dimensionless *locking parameter* corresponding to the lock-up phenomenon such that in the limit $(I_1 - 3) \to J_m$, there is a dramatic rise of the stresses and the material locks up. In the limit $J_m \to \infty$ this model is reduced to the neo-Hookean model, namely

$$\Psi_H = \frac{\mu}{2}(I_1 - 3). \tag{9}$$

The strain energy-density function of a transversely isotropic (TI) material, whose preferred direction in the reference configuration is along the unit vector $\hat{\mathbf{L}}$, depends on two additional invariants

$$I_4 = \hat{\mathbf{L}} \cdot \mathbf{C}\hat{\mathbf{L}} \quad \text{and} \quad I_5 = \hat{\mathbf{L}} \cdot \mathbf{C}^2\hat{\mathbf{L}}. \tag{10}$$

Following Ericksen and Rivlin [13], an alternative set of invariants was proposed in deBotton et al. [12], namely

$$\lambda_n^2 = I_4, \tag{11}$$

$$\lambda_p^2 = \sqrt{\frac{I_3}{I_4}}, \tag{12}$$

$$\gamma_n^2 = \frac{I_5}{I_4} - I_4, \tag{13}$$

$$\gamma_p^2 = I_1 - \frac{I_5}{I_4} - 2\sqrt{\frac{I_3}{I_4}}. \tag{14}$$

The fifth invariant ψ_γ, whose exact expression is given in [12], is the only invariant that depends on I_2. The reverse relations can be readily obtained. The motivation for this set of

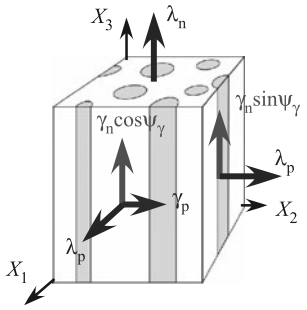

Fig. 1 A scheme of a transversely isotropic composite and the associated physically motivated invariants

invariants stems from the fact that they can be associated with specific modes of deformation. Thus, λ_n is the stretch measure along the preferred direction $\hat{\mathbf{L}}$, λ_p is the measure of the in-plane transverse dilatation, γ_n is the measure of the amount of out-of-plane shear, and γ_p is the amount of shear in the transverse plane. The fifth invariant ψ_γ describes the coupling between the shearing modes. A schematic drawing of the physical interpretation of these invariants is given in Fig. 1.

Following Ogden [32] and Merodio and Ogden [26], we define the tensor of elastic moduli

$$\boldsymbol{\mathcal{A}} = \frac{\partial \mathbf{P}}{\partial \mathbf{F}}. \tag{15}$$

Accordingly, the 1st Piola-Kirchhoff stress increment is

$$\delta \mathbf{P} = \boldsymbol{\mathcal{A}} \delta \mathbf{F}, \tag{16}$$

where $\delta \mathbf{F}$ is an infinitesimal variation in the deformation gradient from the current configuration. If the deformation is homogeneous then $\mathcal{A}_{\alpha i \beta j}$ is independent of $\mathbf{X}$ and the incremental equilibrium equation can be written in the form

$$\mathcal{A}_{\alpha i \beta j} \frac{\partial^2 \delta \chi_j}{\partial X_\alpha \partial X_\beta} = 0, \tag{17}$$

where $\boldsymbol{\delta \chi}$ is the incremental displacement associated with $\delta \mathbf{F}$. For incompressible materials the equilibrium equation is

$$\mathcal{A}_{\alpha i \beta j} \frac{\partial^2 \delta \chi_j}{\partial X_\alpha \partial X_\beta} + \frac{\partial \delta p}{\partial x_i} = 0, \tag{18}$$

where δp is a pressure increment. Incompressibility implies zero divergence of the displacement field, that is

$$\nabla \cdot \boldsymbol{\delta \chi} = 0. \tag{19}$$

We seek a solution for (18) in the form

$$\boldsymbol{\delta \chi} = \hat{\mathbf{m}} \mathrm{e}^{ik\mathbf{x}\cdot\hat{\mathbf{n}}}, \qquad \delta p = q \mathrm{e}^{ik\mathbf{x}\cdot\hat{\mathbf{n}}} \tag{20}$$

where k is a wave number and $\hat{\mathbf{m}}$ and $\hat{\mathbf{n}}$ are two unit vectors.

The incompressibility constraint (19) leads to the requirement

$$\hat{\mathbf{n}} \cdot \hat{\mathbf{m}} = 0. \tag{21}$$

By application of the chain rule, the incremental equilibrium equation (18) can be written in the form

$$\mathcal{A}_{0piqj}\frac{\partial^2\delta\chi_j}{\partial x_p\partial x_q}+\frac{\partial\delta p}{\partial x_i}=0, \tag{22}$$

where

$$\mathcal{A}_{0piqj}=J^{-1}F_{p\alpha}F_{q\beta}\mathcal{A}_{\alpha i\beta j}. \tag{23}$$

Substitution of (20) into (22) results in the equation

$$\mathbf{Q}\hat{\mathbf{m}}+iq\hat{\mathbf{n}}=0, \tag{24}$$

where

$$Q_{ij}\equiv\mathcal{A}_{0piqj}\hat{n}_p\hat{n}_q, \tag{25}$$

is the acoustic tensor.

Finally, we note that the ellipticity condition implies that $Q_{ij}\hat{m}_i\hat{m}_j\neq 0$ for all vectors $\hat{\mathbf{n}}$ and $\hat{\mathbf{m}}$ such that $\hat{\mathbf{n}}\otimes\hat{\mathbf{m}}\neq 0$. However, since negative values of $Q_{ij}\hat{m}_i\hat{m}_j$ are not physical, the strong ellipticity conditions can be written as

$$Q_{ij}\hat{m}_i\hat{m}_j>0. \tag{26}$$

The unit vector $\hat{\mathbf{m}}$ is the normal to a surface, in the deformed configuration, which is referred to as a *weak surface* (e.g., Merodio and Ogden [26]). Once the critical deformation corresponding to the onset of ellipticity loss is achieved, the deformation in the weak surface occurs along the direction of the vector $\hat{\mathbf{n}}$.

3 Fiber Reinforced Composites

The strain energy-density function of a n-phase composite is

$$\Psi(\bar{\mathbf{F}},\mathbf{X})=\sum_{r=1}^{n}\varphi^{(r)}(\mathbf{X})\Psi^{(r)}(\mathbf{F}), \tag{27}$$

where

$$\varphi^{(r)}(\mathbf{X})=\begin{cases}1 & \text{if } \mathbf{X}\in\mathcal{B}_0^{(r)},\\ 0 & \text{otherwise,}\end{cases} \tag{28}$$

and the volume fraction of the r-phase is

$$c^{(r)}=\int_{\mathcal{B}_0}\varphi^{(r)}(\mathbf{X})\,dV. \tag{29}$$

Following the works of Hill [18] and Ogden [31], we apply homogeneous boundary conditions $\mathbf{x}=\mathbf{F}_0\mathbf{X}$ on the boundary of the composite $\partial\mathcal{B}_0$, where $\mathbf{F}_0$ is a constant matrix with $\det\mathbf{F}_0>0$. It can be shown that $\bar{\mathbf{F}}=\mathbf{F}_0$ where

$$\bar{\mathbf{F}}=\frac{1}{V}\int_{\mathcal{B}_0}\mathbf{F}(\mathbf{X})\,dV, \tag{30}$$

is the average deformation gradient. The average 1st Piola-Kirchhoff stress tensor is

$$\bar{\mathbf{P}} = \frac{1}{V}\int_{\mathcal{B}_0} \mathbf{P}(\mathbf{X})\, dV. \tag{31}$$

By application of the principle of minimum energy, the *effective* strain energy-density function is

$$\tilde{\Psi}(\bar{\mathbf{F}}) = \inf_{\mathbf{F}\in\mathcal{K}(\bar{\mathbf{F}})} \left\{ \frac{1}{V}\int_{\mathcal{B}_0} \Psi(\mathbf{F}, \mathbf{X})\, dV \right\}, \tag{32}$$

where $\mathcal{K}(\mathbf{F}) \equiv \{\mathbf{F} \mid \mathbf{F} = \frac{\partial \boldsymbol{\chi}(\mathbf{X})}{\partial \mathbf{X}},\ \mathbf{X} \in \mathcal{B}_0;\ \boldsymbol{\chi}(\mathbf{X}) = \bar{\mathbf{F}}\mathbf{X},\ \mathbf{X} \in \partial\mathcal{B}_0\}$ is the set of kinematically admissible deformation gradients. The corresponding macroscopic constitutive relation is

$$\bar{\mathbf{P}} = \frac{\partial \tilde{\Psi}(\bar{\mathbf{F}})}{\partial \bar{\mathbf{F}}}. \tag{33}$$

Generally, application of the variational principle (32) to heterogeneous materials can lead to bifurcations corresponding to dramatic changes in the nature of the solution to the optimization problem. As discussed by Triantafyllidis and Maker [40] and Geymonat et al. [16], these instabilities may occur at different wavelengths ranging from the size of a typical heterogeneity to that of the entire composite specimen. The calculation of microscopic instabilities at wavelengths that are smaller than the typical size of the specimen is quite complicated, and for periodic microstructures requires analyses of the Bloch wave type. Analysis of macroscopic bifurcations at wave lengths that are comparable with the size of the specimen are accomplished by treating the composite as a homogeneous medium. In this limit usage of the primary solution for (32) is made in conjunction with the procedure outlined in the previous section for determining loss of strong ellipticity. Geymonat et al. [16] further showed that the domain characterizing the onset of macroscopic instabilities is an upper bound for the one characterizing the onset of instabilities at a smaller wavelength. In some cases, however, the macroscopic instabilities are the ones that occur first (e.g., Nestorovic and Triantafyllidis [30]).

In this work the *nonlinear-comparison* (NLC) variational method is used to estimate the effective properties of composites as defined in (32). The method is based on the derivation of a lower bound for the effective strain energy-density function with the aid of an appropriate estimate for the effective strain energy-density function of a non-linear comparison composite (deBotton and Shmuel [11]). The NLC variational estimate for $\tilde{\Psi}(\bar{\mathbf{F}})$ states that

$$\hat{\Psi}(\bar{\mathbf{F}}) = \hat{\Psi}_0(\bar{\mathbf{F}}) + \sum_{r=1}^{n} c^{(r)} \inf_{\mathbf{F}} \left\{ \Psi^{(r)}(\mathbf{F}) - \Psi_0^{(r)}(\mathbf{F}) \right\}, \tag{34}$$

where $\hat{\Psi}_0$ is an estimate for the effective SEDF of a comparison hyperelastic composite whose phases behaviors are governed by the SEDFs $\Psi_0^{(r)}$, and their distributions are characterized by the functions $\varphi^{(r)}$ given in (28). The term appearing in the second part of (34) is denoted the *corrector term*, and we note that it depends only on the properties of the phases of the two composites.

Fiber composites are heterogeneous materials that are commonly made out of stiffer fibers that are embedded in a softer phase. Here we assume that the fibers are all aligned in a particular direction $\hat{\mathbf{L}}$. If we further assume that their distribution in the transverse plane

is random, the overall behavior of the composite is transversely isotropic. We examine two-phase transversely isotopic fiber composites whose phases strain energy-density functions are $\Psi^{(f)}$ and $\Psi^{(m)}$ for the fiber and the matrix phases, respectively. Both $\Psi^{(f)}$ and $\Psi^{(m)}$ are incompressible, isotropic and depend only on I_1. With the aid of the TIH model of deBotton et al. [12] for a neo-Hookean fiber composite as the comparison composite, the NLC estimate for the effective strain energy density function is described by the optimization problem

$$\hat{\Psi}^{(TI)}\left(\bar{\lambda}_p^2, \bar{\lambda}_n^2, \bar{\gamma}_p^2, \bar{\gamma}_n^2\right) = \inf_{\omega}\left(c^{(m)}\Psi^{(m)}\left(\tilde{I}_1^{(m)}\left(\bar{\mathbf{F}}, \hat{\mathbf{L}}, \omega\right)\right) + c^{(f)}\Psi^{(f)}\left(\tilde{I}_1^{(f)}\left(\bar{\mathbf{F}}, \hat{\mathbf{L}}, \omega\right)\right)\right), \quad (35)$$

where

$$\tilde{I}_1^{(r)}(\bar{\mathbf{F}}, \hat{\mathbf{L}}, \omega) = \bar{\lambda}_n^2 + 2\bar{\lambda}_p^2 + \alpha^{(r)}\left(\bar{\gamma}_n^2 + \bar{\gamma}_p^2\right), \quad (36)$$

with

$$\alpha^{(f)} = \left(1 - c^{(m)}\omega\right)^2, \quad (37)$$

and

$$\alpha^{(m)} = \left(1 + c^{(f)}\omega\right)^2 + c^{(f)}\omega^2. \quad (38)$$

The details of the derivation of expression (35) from the NLC variational statement in (34) are given in deBotton and Shmuel [11].

We denote by $\tilde{\omega}$ the value of ω that yields the solution for the Euler-Lagrange equation associated with (35). Clearly, $\tilde{\omega}$ is a function of the average deformation gradient, that is

$$\tilde{\omega} = \tilde{\omega}(\bar{\mathbf{F}}). \quad (39)$$

In some cases $\tilde{\omega}$ can be determined analytically, otherwise it must be calculated numerically. Since the partial derivative of $\hat{\Psi}^{(TI)}$ with respect to ω identically vanishes at $\tilde{\omega}$, the expression for the macroscopic stress can be evaluated analytically without the need for differentiating $\tilde{\omega}$ with respect to $\bar{\mathbf{F}}$. Specifically, the macroscopic nominal stress is

$$\hat{\mathbf{P}} = \sum_{r=m,\,f} c^{(r)} \frac{\partial \hat{\Psi}^{(TI)}}{\partial \tilde{I}_1^{(r)}} \frac{\partial \tilde{I}_1^{(r)}}{\partial \bar{\mathbf{F}}} + p\bar{\mathbf{F}}^{-T}, \quad (40)$$

where

$$\frac{\partial \tilde{I}_1^{(r)}}{\partial \mathbf{F}}(\bar{\mathbf{F}}) = 2\left(\tilde{\alpha}^{(r)}\bar{\mathbf{F}} + (1 - \tilde{\alpha}^{(r)})\left(1 - \frac{\lambda_p^2}{\lambda_n^2}\right)\bar{\mathbf{F}}\hat{\mathbf{L}} \otimes \hat{\mathbf{L}}\right), \quad (41)$$

and $\tilde{\alpha}^{(r)} = \alpha^{(r)}(\tilde{\omega})$.

The corresponding estimate for the tensor of the effective instantaneous elastic moduli can be written as

$$\hat{\mathcal{A}} = \sum_{r=m,\,f}\left(\frac{\partial^2 \hat{\Psi}^{(TI)}}{\partial \tilde{I}_1^{(r)} \partial \tilde{I}_1^{(r)}} \mathbf{S}^{(r)}(\tilde{\omega}, \bar{\mathbf{F}}) \mathbf{S}^{(r)}(\tilde{\omega}, \bar{\mathbf{F}}) + \frac{\partial \hat{\Psi}^{(TI)}}{\partial \tilde{I}_1^{(r)}} \mathcal{G}^{(r)}(\tilde{\omega}, \bar{\mathbf{F}})\right), \quad (42)$$

where

$$\mathbf{S}^{(r)}(\tilde{\omega}, \bar{\mathbf{F}}) = \frac{\partial \tilde{I}_1^{(r)}}{\partial \bar{\mathbf{F}}}(\bar{\mathbf{F}}) + \frac{\partial \tilde{I}_1^{(r)}}{\partial \omega}(\tilde{\omega}) \frac{\partial \tilde{\omega}}{\partial \bar{\mathbf{F}}}, \quad (43)$$

and

$$\mathcal{G}^{(r)}(\tilde{\omega}, \bar{\mathbf{F}}) = \frac{\partial^2 \tilde{I}_1^{(r)}}{\partial \mathbf{F} \partial \mathbf{F}}(\bar{\mathbf{F}}) + 2\frac{\partial \tilde{I}_1^{(r)}}{\partial \omega}(\tilde{\omega})\frac{\partial^2 \tilde{\omega}}{\partial \mathbf{F} \partial \mathbf{F}} + \mathbf{Z}^{(r)}\frac{\partial \tilde{\omega}}{\partial \mathbf{F}} + \left(\mathbf{Z}^{(r)}\frac{\partial \tilde{\omega}}{\partial \mathbf{F}}\right)^T. \tag{44}$$

The first derivatives of $\tilde{I}_1^{(r)}(\bar{\mathbf{F}})$ with respect to $\bar{\mathbf{F}}$ are given in (41), and the first derivatives with respect to ω are

$$\frac{\partial \tilde{I}_1^{(m)}}{\partial \omega}(\tilde{\omega}) = 4c^{(f)}\left(1 + \tilde{\omega} + c^{(f)}\tilde{\omega}\right)\left(\bar{\gamma}_n^2 + \bar{\gamma}_p^2\right), \tag{45}$$

and

$$\frac{\partial \tilde{I}_1^{(f)}}{\partial \omega}(\tilde{\omega}) = -4c^{(m)}\left(1 - c^{(m)}\tilde{\omega}\right)\left(\bar{\gamma}_n^2 + \bar{\gamma}_p^2\right). \tag{46}$$

The second derivative of $\tilde{I}_1^{(r)}(\bar{\mathbf{F}})$ with respect to $\bar{\mathbf{F}}$ in (44) is

$$\frac{\partial^2 \tilde{I}_1^{(r)}}{\partial \bar{F}_{ij} \partial \bar{F}_{kl}}(\bar{\mathbf{F}}) = 2\left(\tilde{\alpha}^{(r)}\delta_{ik}\delta_{jl} + \left(1 - \tilde{\alpha}^{(r)}\right)\left(\left(1 - \frac{\bar{\lambda}_p^2}{\bar{\lambda}_n^2}\right)\delta_{ik} + \frac{3\bar{\lambda}_p^2}{\bar{\lambda}_n^4}\bar{F}_{ip}\bar{F}_{ks}\hat{L}_s\hat{L}_p\right)\hat{L}_l\hat{L}_j\right). \tag{47}$$

The terms $\mathbf{Z}^{(r)}$ in (44) are

$$\mathbf{Z}^{(m)} = 4c^{(f)}\left(1 + \tilde{\omega} + c^{(f)}\tilde{\omega}\right)\left(\bar{\mathbf{F}} - \left(1 - \frac{\bar{\lambda}_p^2}{\bar{\lambda}_n^2}\right)\bar{\mathbf{F}}\hat{\mathbf{L}} \otimes \hat{\mathbf{L}}\right) \tag{48}$$

and

$$\mathbf{Z}^{(f)} = -4c^{(m)}\left(1 - c^{(m)}\tilde{\omega}\right)\left(\bar{\mathbf{F}} - \left(1 - \frac{\bar{\lambda}_p^2}{\bar{\lambda}_n^2}\right)\bar{\mathbf{F}}\hat{\mathbf{L}} \otimes \hat{\mathbf{L}}\right). \tag{49}$$

Note that the terms that do not include derivatives of $\tilde{\omega}(\bar{\mathbf{F}})$ with respect to $\bar{\mathbf{F}}$ can be evaluated a priori with substitution of $\tilde{\omega}$ after the solution of the optimization problem is obtained either analytically or numerically. Additionally,

$$\frac{\partial \tilde{\omega}}{\partial \bar{\mathbf{F}}} = \frac{\partial \tilde{\omega}}{\partial \lambda_n^2}\frac{\partial \bar{\lambda}_n^2}{\partial \bar{\mathbf{F}}} + \frac{\partial \tilde{\omega}}{\partial \lambda_p^2}\frac{\partial \bar{\lambda}_p^2}{\partial \bar{\mathbf{F}}} + \frac{\partial \tilde{\omega}}{\partial \gamma_n^2}\frac{\partial \bar{\gamma}_n^2}{\partial \bar{\mathbf{F}}} + \frac{\partial \tilde{\omega}}{\partial \gamma_p^2}\frac{\partial \bar{\gamma}_p^2}{\partial \bar{\mathbf{F}}}, \tag{50}$$

and

$$\begin{aligned}\frac{\partial^2 \tilde{\omega}}{\partial \bar{\mathbf{F}} \partial \bar{\mathbf{F}}} = {} & \frac{\partial^2 \tilde{\omega}}{\partial \lambda_n^2 \partial \bar{\mathbf{F}}}\frac{\partial \bar{\lambda}_n^2}{\partial \bar{\mathbf{F}}} + \frac{\partial \tilde{\omega}}{\partial \lambda_n^2}\frac{\partial^2 \bar{\lambda}_n^2}{\partial \bar{\mathbf{F}} \partial \bar{\mathbf{F}}} + \frac{\partial^2 \tilde{\omega}}{\partial \lambda_p^2 \partial \bar{\mathbf{F}}}\frac{\partial \bar{\lambda}_p^2}{\partial \bar{\mathbf{F}}} + \frac{\partial \tilde{\omega}}{\partial \lambda_p^2}\frac{\partial^2 \bar{\lambda}_p^2}{\partial \bar{\mathbf{F}} \partial \bar{\mathbf{F}}} \\ & + \frac{\partial^2 \tilde{\omega}}{\partial \gamma_n^2 \partial \bar{\mathbf{F}}}\frac{\partial \bar{\gamma}_n^2}{\partial \bar{\mathbf{F}}} + \frac{\partial \tilde{\omega}}{\partial \gamma_n^2}\frac{\partial^2 \bar{\gamma}_n^2}{\partial \bar{\mathbf{F}} \partial \bar{\mathbf{F}}} + \frac{\partial^2 \tilde{\omega}}{\partial \gamma_p^2 \partial \bar{\mathbf{F}}}\frac{\partial \bar{\gamma}_p^2}{\partial \bar{\mathbf{F}}} + \frac{\partial \tilde{\omega}}{\partial \gamma_p^2}\frac{\partial^2 \bar{\gamma}_p^2}{\partial \bar{\mathbf{F}} \partial \bar{\mathbf{F}}},\end{aligned} \tag{51}$$

where the explicit expressions for the derivatives of the invariants $\bar{\lambda}_n^2$, $\bar{\lambda}_p^2$, $\bar{\gamma}_n^2$, and $\bar{\gamma}_p^2$ are given in Appendix. We note that, in general, the derivatives of $\tilde{\omega}$ with respect to $\bar{\lambda}_n^2$, $\bar{\lambda}_p^2$, $\bar{\gamma}_n^2$, and $\bar{\gamma}_p^2$ must be determined numerically unless an analytical solution for the optimization problem (35) can be derived. Finally, once the elastic moduli tensor (42) is determined, the strong ellipticity condition (26) can be checked.

When both phases of the composite are neo-Hookean, the optimization problem (35) yields

$$\tilde{\omega}^{(H)} = \frac{\mu^{(f)} - \mu^{(m)}}{c^{(m)}\mu^{(f)} + (1 + c^{(f)})\mu^{(m)}}, \tag{52}$$

and the effective strain energy density function takes the form introduced by deBotton et al. [12],

$$\hat{\Psi}^{TIH} = \bar{\mu}\left(\bar{\lambda}_n^2 + 2\bar{\lambda}_p^2 - 3\right) + \tilde{\mu}_p\bar{\gamma}_p^2 + \tilde{\mu}_n\bar{\gamma}_n^2, \tag{53}$$

where

$$\tilde{\mu}_p = \tilde{\mu}_n = \tilde{\mu} = \mu^{(m)}\frac{(1 + c^{(f)})\mu^{(f)} + (1 - c^{(f)})\mu^{(m)}}{(1 - c^{(f)})\mu^{(f)} + (1 + c^{(f)})\mu^{(m)}}, \tag{54}$$

is the expression for both the in-plane shear $\tilde{\mu}_p$ (deBotton [7]), and the out-of-plane shear $\tilde{\mu}_n$ (deBotton and Hariton [8]), and

$$\bar{\mu} = c^{(f)}\mu^{(f)} + c^{(m)}\mu^{(m)}, \tag{55}$$

is the isochoric shear modulus (e.g., deBotton et al.. [12], He et al. [17]). More recently Lopez-Pamies and Idiart [23] extended the work of deBotton [7] and demonstrated that (53) is an *exact* expression for the effective strain energy-density function of neo-Hookean sequentially-coated laminates. The tensor of elastic moduli associated with the strain energy-density function (53) together with (54) is

$$\mathcal{A}_{ijkl} = \tilde{\mu}\delta_{ik}\delta_{jl} + (\bar{\mu} - \tilde{\mu})\left(\frac{3\bar{\lambda}_p^2}{\bar{\lambda}_n^4}\bar{F}_{ip}\bar{F}_{ks}\hat{L}_s\hat{L}_p + \left(1 - \frac{\bar{\lambda}_p^2}{\bar{\lambda}_n^2}\right)\delta_{ik}\right)\hat{L}_l\hat{L}_j. \tag{56}$$

Applying the strong ellipticity condition (26) a simple expression for the critical compressive stretch ratio in the fiber direction is obtained, namely

$$\bar{\lambda}_n = \left(1 - \frac{\tilde{\mu}}{\bar{\mu}}\right)^{1/3}. \tag{57}$$

We note that Agoras et al. [2] derived expressions (56) and (57) from the SEDF $\hat{\Psi}^{TIH}$ of deBotton et al. [12]. These investigators also derived the corresponding expressions that result from the LC variational method for composites with neo-Hookean phases. Under compression along the fibers both methods lead to expression (57), however for more general loading conditions the expression resulting from the LC method is more complicated than (56) and requires a solution of a quartic polynomial in parallel with (26). Agoras et al. [2] computed the onset of ellipticity loss under general loading conditions and found that in some cases the predictions of the LC variational estimate are in agreement with the predictions resulting from the SEDF $\hat{\Psi}^{TIH}$ that corresponds to a *realizable* composite.

As was mentioned in the introduction, Agoras et al. [2] also determined estimates for the onset of instabilities in fiber composites with Gent phases by application of the LC variational estimate. For this class of composites the resulting expressions are more involved and require a solution of two nonlinear equations in conjunction with the strong ellipticity condition (26). Contrarily, even with Gent phases the optimization problem stemming from the NLC variational estimate of deBotton and Shmuel [11] can be solved *analytically* to end up with an *explicit estimate* for the effective SEDF. In particular, the resulting Euler-Lagrange

equations admit the form of a cubic polynomial in ω, from which explicit analytical expressions for $\tilde{\omega}$ and $\mathcal{A}_{ijkl}$ are obtained. For later reference we note that

$$\tilde{\omega}^{(G)} = \tilde{\omega}^{(G)}\left(\bar{\mathbf{F}},\, c^{(f)},\, k,\, \mu^{(m)},\, t,\, J_m^{(m)}\right), \tag{58}$$

where

$$k = \mu^{(f)}/\mu^{(m)}, \tag{59}$$

is the ratio between the initial shear moduli of the fiber and the matrix, and

$$t = J_m^{(f)}/J_m^{(m)}, \tag{60}$$

is the ratio between the locking parameters.

We emphasize that the analytical procedure described so far can be used to estimate the macroscopic stable domains of hyperelastic fiber composites under general loading conditions. However, in the sequel we restrict our attention to plane-strain loading condition where the constrained direction of the deformation is normal to the direction of the fibers (e.g., Qiu and Pence [37]). This allows to examine the onset of instabilities due to compression along the fibers and to compare the analytical predictions with corresponding finite element simulations.

For convenience, we distinguish between the *principal* coordinate system of the right Cauchy-Green deformation tensor and the *material* coordinate system. Without loss of generality we define the material coordinate system such that in the reference state the direction of the fiber $\hat{\mathbf{L}}$ is aligned with the X_3-axis (see Fig. 1). Specifically, we set $F_{11} = 1$. Note, that with this choice the X_1-axis is common for both the principal and the material systems. Accordingly, in the principal coordinate system the plane-strain average deformation gradient is

$$\bar{\mathbf{F}}' = \begin{pmatrix} 1 & 0 & 0 \\ 0 & \bar{\lambda}^{-1} & 0 \\ 0 & 0 & \bar{\lambda} \end{pmatrix}. \tag{61}$$

This is related to the average deformation gradient in the material coordinate system via the relation

$$\bar{\mathbf{F}} = \mathbf{R}^T \bar{\mathbf{F}}' \mathbf{R}, \tag{62}$$

where

$$\mathbf{R} = \begin{pmatrix} 1 & 0 & 0 \\ 0 & \cos\Theta & \sin\Theta \\ 0 & -\sin\Theta & \cos\Theta \end{pmatrix}, \tag{63}$$

is a rotation tensor. Here Θ is the referential angle between the direction of the principal stretch and the fiber direction.

In accordance with the plane-strain assumption, we also restrict the solution of (20) with a choice of infinitesimal planar deformation along the vectors $\hat{\mathbf{n}} = (0,\, \cos\phi,\, \sin\phi)$ and $\hat{\mathbf{m}} = (0,\, \sin\phi,\, -\cos\phi)$. While this choice of deformation is consistent with the plane-strain assumption, on physical grounds a choice of non-planar infinitesimal deformation is admissible. For instance, the solution ensued from this choice coincides with the solution obtained by Agoras et al. [2] with the choice $\hat{\mathbf{n}} = (0,\, 1,\, 0)$ and $\hat{\mathbf{m}} = (\sin\phi,\, 0,\, -\cos\phi)$.

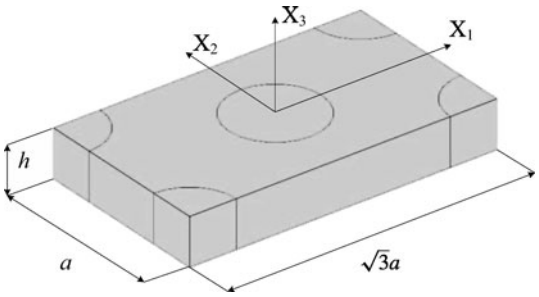

Fig. 2 The hexagonal unit cell modeled in the finite element code COMSOL

4 Finite Element Simulation

We construct 3-D finite element models of fiber composites to estimate their macroscopic behaviors and stability regimes. We also construct 2-D laminated models as basis for comparison since these models are frequently being used for estimation of the onset of failures in fiber composites. We note that the analytical treatment considered in the previous section corresponded to fiber composites with transversely isotropic symmetry. Khisaeva and Ostoja-Starzewski [21] and Moraleda et al. [29] considered periodic FE models with a few tenth of fibers in the unit cell in order to approximate the macroscopically isotropic response of TI composites in the transverse plane. In this work we consider the less computationally extensive model of periodic composites with hexagonal unit cell. These materials are orthotropic materials, however, in the limit of infinitesimal deformations they behave like transversely isotropic materials. This property makes them fair candidates for comparison with our analytical results (e.g., Aravas et al. [3], Michel et al. [28], Shmuel and deBotton [39]). This is particularly relevant in the context of instabilities due to compression along the fibers since the critical stretch ratios are usually larger than 0.95. We further note that in the loading modes that we consider in this work (compression and out-of-plane shear along the fibers) the precise distribution of the fibers in the transverse plane is not a crucial parameter.

A representative 3-D unit cell of a periodic composite with hexagonal arrangement of the fibers is shown in Fig. 2. The fibers are aligned along the X_3 axis and the ratio between the long to the short faces in the transverse plane is $\sqrt{3}$. The unit cell occupies the domain

$$-\frac{\sqrt{3}a}{2} \leq X_1 \leq \frac{\sqrt{3}a}{2}, \qquad -\frac{a}{2} \leq X_2 \leq \frac{a}{2}, \qquad -\frac{h}{2} \leq X_3 \leq \frac{h}{2}, \tag{64}$$

in the reference configuration. The response of the composite is obtained by applying periodic displacement boundary conditions and determining the average stress field in the unit cell from the resulting traction on the boundaries. The boundary conditions are extracted from the average deformation gradient tensor in (62) and imposed on the six faces of the unit cell as follows:

(1) The top ($X_3 = \frac{h}{2}$) and bottom ($X_3 = -\frac{h}{2}$) faces are related via

$$\begin{cases} u_1^B = u_1^T + \bar{F}_{13}h, \\ u_2^B = u_2^T + \bar{F}_{23}h, \\ u_3^B = u_3^T + (\bar{F}_{33} - 1)h. \end{cases} \tag{65}$$

(2) The front ($X_2 = \frac{a}{2}$) and rear ($X_2 = -\frac{a}{2}$) faces are related via

$$\begin{cases} u_1^F = u_1^{Re} + \bar{F}_{12}a, \\ u_2^F = u_2^{Re} + (\bar{F}_{22} - 1)a, \\ u_3^F = u_3^{Re} + \bar{F}_{32}a. \end{cases} \tag{66}$$

(3) The right ($X_1 = \frac{a\sqrt{3}}{2}$) and left ($X_1 = -\frac{a\sqrt{3}}{2}$) faces are related via

$$\begin{cases} u_1^L = u_1^R + (\bar{F}_{11} - 1)a\sqrt{3}, \\ u_2^L = u_2^R + \bar{F}_{21}a\sqrt{3}, \\ u_3^L = u_3^R + \bar{F}_{31}a\sqrt{3}. \end{cases} \tag{67}$$

The analysis of loss of ellipticity requires determination of the instantaneous tensor of elastic moduli. To this end we perform a set of additional incremental deformations from the deformed configuration. These incremental deformations lead to a macroscopic response of the model and result in an incremental variation of the average nominal stress. By making use of relation (16) in the principal coordinate system we obtain the expression

$$\delta\bar{\mathbf{P}}' = \bar{\boldsymbol{\mathcal{A}}}'\delta\bar{\mathbf{F}}', \tag{68}$$

from which the instantaneous macroscopic elastic moduli are estimated. When the deformation gradient is restricted to the planar form of (62), there is no deformation in the X_1 direction and the following three plane tests can be performed, namely

$$\bar{\mathbf{F}}'^{(1)} = \begin{pmatrix} 1 & 0 & 0 \\ 0 & \bar{\lambda}^{-1} & \delta\bar{\gamma} \\ 0 & 0 & \bar{\lambda} \end{pmatrix}, \qquad \bar{\mathbf{F}}'^{(2)} = \begin{pmatrix} 1 & 0 & 0 \\ 0 & \bar{\lambda}^{-1} & 0 \\ 0 & \delta\bar{\gamma} & \bar{\lambda} \end{pmatrix}, \tag{69}$$

and the biaxial test

$$\bar{\mathbf{F}}'^{(3)} = \begin{pmatrix} 1 & 0 & 0 \\ 0 & (\bar{\lambda} + \delta\bar{\lambda})^{-1} & 0 \\ 0 & 0 & \bar{\lambda} + \delta\bar{\lambda} \end{pmatrix}, \tag{70}$$

where $\delta\bar{\gamma}$ and $\delta\bar{\lambda}$ are small increments. The deformation gradient and the nominal stress tensor increments in the principal coordinate system are

$$\delta\bar{\mathbf{F}}'^{(i)} = \bar{\mathbf{F}}'^{(i)} - \bar{\mathbf{F}}' \quad \text{and} \quad \delta\bar{\mathbf{P}}'^{(i)} = \bar{\mathbf{P}}'^{(i)} - \bar{\mathbf{P}}', \tag{71}$$

respectively.

We note that it is impossible to fully characterize the elastic properties of transversely isotropic materials on the basis of plane tests alone (e.g., Ogden [33]). This means that we cannot determine some of the terms of the tensor of macroscopic elastic moduli. Nonetheless, the condition for the loss of ellipticity can be extracted from appropriate *combinations* of the terms of the elastic tensor obtained from the planar tests. Specifically, the strong ellipticity condition (26), rewritten in the principal coordinate system of the left Cauchy-Green strain tensor, together with the incompressibility constraint (21) is

$$\begin{aligned} &\left((\bar{\mathcal{A}}'_{0\,3333} - \bar{\mathcal{A}}'_{0\,3322}) + (\bar{\mathcal{A}}'_{0\,2222} - \bar{\mathcal{A}}'_{0\,3322}) - 2\bar{\mathcal{A}}'_{0\,2332}\right) n_3^2 n_2^2 + \bar{\mathcal{A}}'_{0\,3232} n_3^4 \\ &\quad + \bar{\mathcal{A}}'_{0\,2323} n_2^4 + 2\left((\bar{\mathcal{A}}'_{0\,2232} - \bar{\mathcal{A}}'_{0\,3332}) n_3^3 n_2 + (\bar{\mathcal{A}}'_{0\,3323} - \bar{\mathcal{A}}'_{0\,2223}) n_2^3 n_3\right) > 0. \end{aligned} \tag{72}$$

Though the individual terms $\bar{\mathcal{A}}'_{0\,3333}$, $\bar{\mathcal{A}}'_{0\,3322}$ and $\bar{\mathcal{A}}'_{0\,2222}$ cannot be determined, the combinations $(\bar{\mathcal{A}}'_{0\,3333}-\bar{\mathcal{A}}'_{0\,3322})$ and $(\bar{\mathcal{A}}'_{0\,2222}-\bar{\mathcal{A}}'_{0\,3322})$ can be extracted from the biaxial plane test (70) by making use of (68), (23) and the incremental incompressibility condition

$$\delta\mathbf{F}:\mathbf{F}^{-T}=0. \tag{73}$$

Thus,

$$\delta\bar{F}'_{22}=-\delta\bar{F}'_{33}\frac{\bar{F}'_{22}}{\bar{F}'_{33}}=-\frac{\delta\bar{F}'_{33}}{\bar{F}'^{2}_{33}}. \tag{74}$$

Applying the biaxial test deformation $\bar{\mathbf{F}}'^{(3)}$, and using relation (23) together with (74), we end up with

$$\begin{aligned}\bar{\mathcal{A}}'_{0\,3333}-\bar{\mathcal{A}}'_{0\,3322}&=\bar{F}'_{33}\bar{F}'_{33}\bar{\mathcal{A}}'_{3333}-\bar{F}'_{33}\bar{F}'_{22}\bar{\mathcal{A}}'_{3322}\\&=\bar{F}'_{33}\bar{F}'_{33}\left(\bar{\mathcal{A}}'_{3333}-\bar{\mathcal{A}}'_{3322}\frac{\bar{F}'_{22}}{\bar{F}'_{33}}\right)=\bar{F}'_{33}\bar{F}'_{33}\frac{\delta\bar{P}'^{(3)}_{33}}{\delta\bar{F}'^{(3)}_{33}},\end{aligned} \tag{75}$$

and

$$\begin{aligned}\bar{\mathcal{A}}'_{0\,2222}-\bar{\mathcal{A}}'_{0\,3322}&=\bar{F}'_{22}\bar{F}'_{22}\bar{\mathcal{A}}'_{2222}-\bar{F}'_{33}\bar{F}'_{22}\bar{\mathcal{A}}'_{3322}\\&=\bar{F}'_{22}\bar{F}'_{22}\left(\bar{\mathcal{A}}'_{2222}-\bar{\mathcal{A}}'_{3322}\frac{\bar{F}'_{33}}{\bar{F}'_{22}}\right)=\bar{F}'_{22}\bar{F}'_{22}\frac{\delta\bar{P}'^{(3)}_{22}}{\delta\bar{F}'^{(3)}_{22}}.\end{aligned} \tag{76}$$

The rest of the terms, namely, $\bar{\mathcal{A}}'_{0\,3323}$, $\bar{\mathcal{A}}'_{0\,2223}$, $\bar{\mathcal{A}}'_{0\,2232}$, $\bar{\mathcal{A}}'_{0\,3332}$, $\bar{\mathcal{A}}'_{0\,3232}$ and $\bar{\mathcal{A}}'_{0\,2323}$ are obtained directly from the shear tests (69) by using (68) and (23).

The simulations were carried out by application of the commercial FE code COMSOL. The deformation is defined in the principal coordinate system in terms of $\bar{\mathbf{F}}'$, and we make use of (62) to impose the boundary conditions (65)–(67) on the unit cell in the material coordinate system where the FE simulation is executed. Next, the resulting output, in terms of the mean nominal stress tensor, is transformed back to the principal coordinate system via the relation

$$\bar{\mathbf{P}}'=\mathbf{R}\bar{\mathbf{P}}\mathbf{R}^{T}. \tag{77}$$

An identical procedure was used to simulate the 2-D models for the laminated composites.

Compressible SEDFs were defined directly in COMSOL code. The neo-Hookean strain energy-density functions of the phases are

$$\Psi_{H}^{(r)}=\frac{\mu^{(r)}}{2}\left(J_1-3\right)+\kappa^{(r)}\left(J-1\right)^2, \tag{78}$$

where $J_1=J^{-2/3}I_1$ and κ is a bulk modulus. The Gent strain energy-density functions are

$$\Psi_{G}^{(r)}=-\frac{\mu^{(r)}}{2}J_m^{(r)}\ln\left(1-\frac{I_1-3}{J_m^{(r)}}\right)-\mu^{(r)}\ln J^{(r)}+\left(\frac{\kappa^{(r)}-2\mu^{(r)}/3}{2}-\frac{\mu^{(r)}}{J_m^{(r)}}\right)\left(J^{(r)}-1\right)^2. \tag{79}$$

Incompressibility was approximated by choosing bulk modulus $\kappa^{(r)}$ in each phase that is two orders of magnitude larger than the corresponding shear modulus $\mu^{(r)}$. A component of the average nominal stress on a given face of the unit cell is calculated by summing

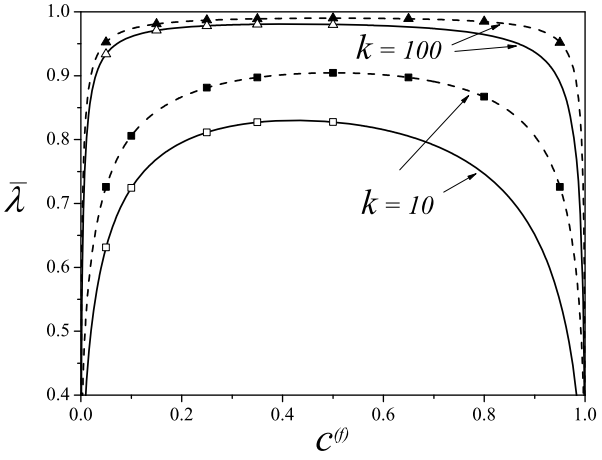

Fig. 3 The dependence of the critical stretch ratio on the fiber volume fraction. The *solid curves* correspond to fiber composites and the *dashed curves* to laminated composites. The results of the numerical simulations are marked by *triangles* for $k = 100$ and *squares* for $k = 10$

the corresponding components of the internal forces acting on the nodes of that face and dividing the resultant force by the area of the face in the undeformed configuration.

5 Applications

We make use of the results of the previous sections to determine numerical and analytical estimates for the loss of stability of fiber composites with neo-Hookean and Gent phases. First, we examine the case when both phases are neo-Hookean. When the composite is compressed along the fibers (i.e., $\Theta = 0$ in (63)) the analytical expression for the critical stretch ratio is given in (57). The corresponding predictions obtained for composites with two different contrasts between the shear moduli of the phases are shown in Fig. 3 as functions of the fiber volume fraction. The solid curves correspond to $k = 100$ and 10.

The corresponding expression for laminated composites that was obtained by Triantafyllidis and Maker [40] is

$$\bar{\lambda}_c = \left(1 - \frac{\hat{\mu}}{\bar{\mu}}\right)^{1/4}, \tag{80}$$

where

$$\hat{\mu} = \left(\frac{c^{(m)}}{\mu^{(m)}} + \frac{c^{(f)}}{\mu^{(f)}}\right)^{-1}, \tag{81}$$

and in this case $\mu^{(f)}$ and $\mu^{(m)}$ are shear moduli of the stiffer and the softer layers, respectively. For comparison, the predictions of this solution are presented in Fig. 3 by the dashed curves for $k = 100$ and 10. The corresponding results of the numerical simulations are marked by triangles for $k = 100$ and squares for $k = 10$. In all cases the numerical results are in excellent agreement with the analytical ones for both the laminated and the fiber composites.

We note that under these loading conditions $\phi = \pi/2$ (i.e., $\hat{\mathbf{m}} = \hat{\mathbf{L}}$), meaning that at the onset of the instability the weak surface is perpendicular to the fibers and the deformation occurs along this surface. As was mentioned in Agoras et al. [2], in agreement with experimental findings this instability is associated with vanishing shear response in the plane

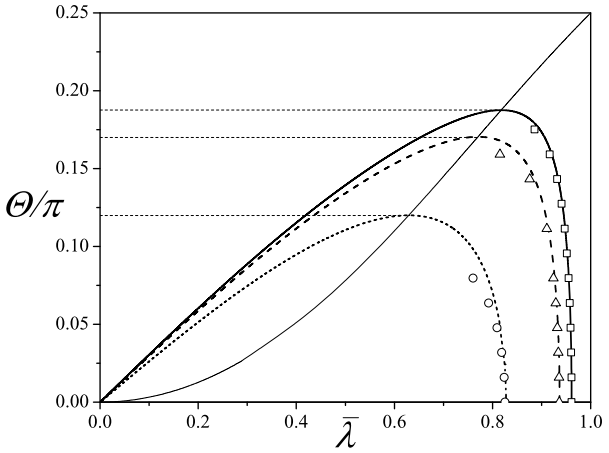

Fig. 4 The dependence of the critical stretch ratio on the loading direction. The *solid*, *dashed and short-dash curves* correspond to composites with fiber to matrix shear moduli ratio $k = 50$, 30 and 10, respectively. The simulation results are marked by *squares*, *triangles* and *circles* for $k = 50$, 30 and 10, respectively. The thin *continuous curve* shows the maximal loading angle Θ_m at which instability may occur. For all curves $c^{(f)} = 0.5$

transverse to the fibers. This observation is also in agreement with the earlier findings of Qiu and Pence [37] and Merodio and Ogden [26].

In comparison with composites with intermediate volume fraction of fibers, the onset of ellipticity loss occurs much later in composites with low and high fiber volume fractions. As expected, the composites become more sensitive to compression as the ratio between the shear moduli increases. A comparison between the results for the laminated and the fiber composites reveals that the stable domain for the fiber composites is larger than the one for the laminated composite, though the trends of the curves are similar. In contrast with the results for the laminated composites, the results for the fiber composite are not symmetric with respect to $c^{(f)} = 0.5$. Thus, at low fiber volume fraction, the composite is more sensitive to compression than at high fiber volume fraction.

A few representative results for the critical stretch ratio under non-aligned compression are shown in Fig. 4. The corresponding expression for $\bar{\lambda}_c$ was determined by Agoras et al. [2] for the TIH model introduced in [12] in terms of the quartic polynomial equation

$$\bar{\lambda}_c^4 \cos^2\Theta - \bar{\lambda}_c^2 \left(1 - \frac{\tilde{\mu}}{\bar{\mu}}\right)^{2/3} + \sin^2\Theta = 0. \tag{82}$$

The solid, dashed and short-dashed curves correspond to fiber to matrix shear moduli ratio $k = 50$, 30 and 10, respectively. In all cases the volume fraction of the fiber is $c^{(f)} = 0.5$. The results of the corresponding numerical simulations are marked by squares, triangles and circles for $k = 50$, 30 and 10, respectively. The curves are symmetric with respect to the loading direction $\Theta = 0$, that is $\bar{\lambda}_c(\Theta) = \bar{\lambda}_c(-\Theta)$, and are also π-periodic, that is, $\bar{\lambda}_c(\Theta) = \bar{\lambda}_c(\Theta + \pi j)$, $j = 1, 2, 3, \ldots$. Additionally we note that $\bar{\lambda}_c(\Theta) = 1/\bar{\lambda}_c(\Theta + \pi/2)$.

Comparing the analytical solution to the numerical simulations, we observe a better agreement for higher shear moduli ratios k. However, for all cases the characteristic behavior is similar and the analytical solution is the more conservative estimation for the onset of failure. The reason for the difference is related to the fact that the analytical solution is obtained for incompressible composites while in the FE simulations the phases are slightly compressible. We emphasize that a decrease in the compressibility of the phases, in terms of an increase in the bulk to shear moduli ratio, resulted in an earlier onset of ellipticity loss and hence to a better agreement between the two estimates. This influence of incompressibility on the onset of failure is in agreement with the observation of Triantafyllidis et al.

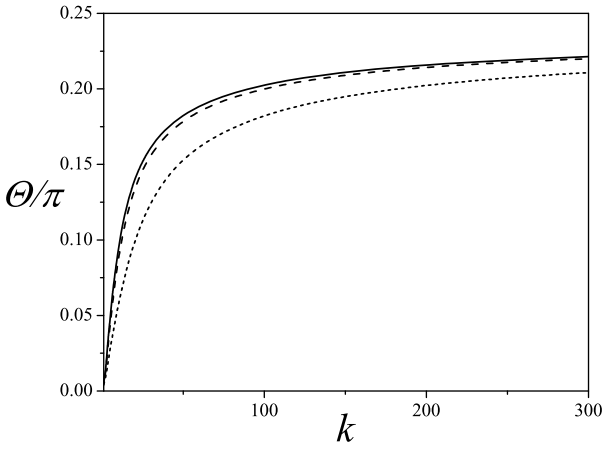

Fig. 5 The dependence of the maximal loading direction angle on the ratio between the shear moduli. The *solid*, *dashed* and *short-dash* curves correspond to volume fractions of the fiber $c^{(f)} = 0.1$, 0.25 and 0.5, respectively

[41]. Additionally, we recall that the microstructure used in the numerical simulation, while providing a fair estimate for composites with randomly distributed fibers, is not an actual TI material.

In consistent with expectations, the value of $\bar{\lambda}_c$ approaches unity asymptotically as $k \to \infty$. Note that as the angle between the loading and the fiber directions increases there exist an angle (Θ_m) beyond which no macroscopic instability occurs. The critical stretch ratio corresponding to this angle is

$$\bar{\lambda}_m = \frac{1}{\sqrt{2}\cos\Theta_m}\left(1 - \frac{\tilde{\mu}}{\bar{\mu}}\right)^{1/3}, \tag{83}$$

and it is represented in Fig. 4 by the thin continuous curve. Obviously, Θ_m depends on the fiber volume fraction and shear moduli ratio, and from (82) it is easy to see that

$$\Theta_m = \frac{1}{2}\arcsin\left(1 - \frac{\tilde{\mu}}{\bar{\mu}}\right)^{2/3}. \tag{84}$$

The dependence of the maximal angle Θ_m on the ratio between the shear moduli is shown in Fig. 5 for fiber volume fractions $c^{(f)} = 0.5$, 0.25 and 0.1 by solid, dashed, and short-dashed curves, respectively. The domain above the curve is the one for which no instability was detected, while in the region beneath the curve critical stretch ratios corresponding to ellipticity loss were found. Obviously, when the shear moduli contrast k becomes large the load direction Θ_m tends to $\pi/4$, corresponding to a switch of the load along the fibers from compression to tension. Combining (83) and (84) we end up with the expression

$$\Theta_m = \arctan\bar{\lambda}_m^2. \tag{85}$$

The physical reasoning for this value becomes clear when we follow the rotation of the fibers under non-aligned load (e.g., deBotton and Shmuel [10]). Thus, in the deformed configuration the angle between the fiber and the loading directions is

$$\theta = \arctan\left(\bar{\lambda}^{-2}\tan\Theta\right). \tag{86}$$

Equations (85) and (86) lead to $\theta_m = \pi/4$. At this angle the loading on the fibers switches from compression to tension. Consequently, beyond this point no instability is detected.

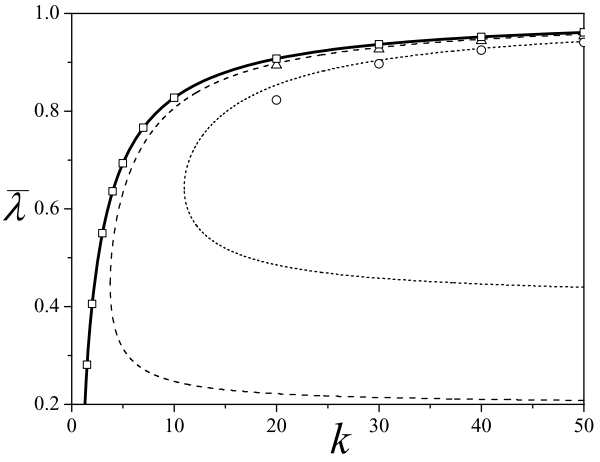

Fig. 6 The critical stretch ratio as a function of the contrast between the phases shear moduli for different loading directions. The *continuous*, *dash* and *short-dashed curves* correspond to $\Theta = 0$, $\pi/16$ and $\pi/8$, respectively. The results of the numerical simulation are marked by *squares*, *triangles* and *circles* for $\Theta = 0$, $\pi/16$ and $\pi/8$, respectively

Thus, we find that the maximal loading angle Θ_m corresponds to the state at which in the *current configuration* $\theta(\bar{\lambda}_c) = \pi/4$.

The dependence of the critical stretch on the contrast between the fiber to the matrix shear moduli is presented in Fig. 6 for different loading directions. The solid, dashed and short-dashed curves correspond to the analytical solution for $\Theta = 0$, $\pi/16$ and $\pi/8$, respectively. The numerical simulation results are presented by squares, triangles and circles for $\Theta = 0$, $\pi/16$ and $\pi/8$, respectively.

The numerical simulation results are in good agreement with the analytical solution for low values of the loading angles. However, for relatively high values of this angle the deformation needed for the onset of ellipticity loss increases and hence the effect of the phases compressibility becomes significant. This, in turn, results in an increase in the difference between the analytical and the numerical predictions. This is on top of the difference stemming from the different microstructures associated with the two estimations.

Next, we examine the responses of composites whose phases behaviors are described by the Gent model (8). As was mentioned before, the variational estimate applied to this model results in a close-form solution of (39) in terms of a cubic polynomial. With this solution, the tensor of elastic moduli $\hat{\boldsymbol{\mathcal{A}}}$ given by (42) is evaluated at each step of the loading path which is described by the loading parameters $\bar{\lambda}$ and Θ. When the left-hand side of (26) becomes non-positive, instability may occur.

Remarkably, we find that for a wide range of materials and loading parameters ($\bar{\lambda}$, Θ, k, $\mu^{(m)}$, $c^{(f)}$, t, $J_m^{(m)}$) the value of $\tilde{\omega}^{(G)}$, the solution of the optimization problem (35), is very close to $\tilde{\omega}^{(H)}$ which is the corresponding solution for the neo-Hookean composite given in (52). Upon substitution of this expression in (35) we end up with the following upper estimate (UE) for $\hat{\Psi}^{(TI)}$, namely,

$$\hat{\Psi}^{(UE)} = -\frac{1}{2}\sum_{r=m,\,f} c^{(r)}\mu^{(r)}J_m^{(r)}\ln\left(1-\frac{\tilde{I}_1^{(r)}(\tilde{\omega}^{(H)})-3}{J_m^{(r)}}\right). \tag{87}$$

Moreover, we find that for a large range of materials and loading parameters the derivatives of $\tilde{\omega}^{(G)}$ with respect to $\bar{\mathbf{F}}$ are negligible and hence not only the stresses can be analytically derived from (87), but also the tensor of elastic moduli can be easily derived. Thus, we have

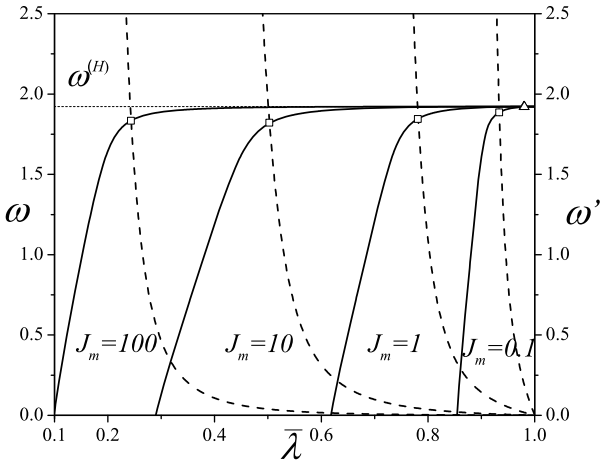

Fig. 7 The dependence of $\tilde{\omega}^{(G)}$ and $(\tilde{\omega}^{(G)})'$ on the stretch ratio $\bar{\lambda}$ for the Gent composite with $\Theta = 0$, $c^{(f)} = 0.5$, $k = 100$ and $t = 1$. The *continuous curves* correspond to $\tilde{\omega}^{(G)}(\bar{\lambda})$ for $J_m = 0.1,\ 1,\ 10,\ 100$ *from right to left*, while the *dashed curves* to $(\tilde{\omega}^{(G)})'(\bar{\lambda})$. The *thin short-dash line* corresponds to $\tilde{\omega}^{(H)}$ for the neo-Hookean composite. The *curve crossings* are marked by *squares*. The *triangle* indicates the critical stretch ratio for these composites

that

$$\hat{\mathcal{A}}^{(UE)} = \sum_{r=m,\,f} \left(\frac{\partial^2 \hat{\Psi}^{(UE)}}{\partial \tilde{I}_1^{(r)} \partial \tilde{I}_1^{(r)}} \frac{\partial \tilde{I}_1^{(r)}}{\partial \bar{\mathbf{F}}}(\bar{\mathbf{F}}) \frac{\partial \tilde{I}_1^{(r)}}{\partial \bar{\mathbf{F}}}(\bar{\mathbf{F}}) + \frac{\partial \hat{\Psi}^{(UE)}}{\partial \tilde{I}_1^{(r)}} \frac{\partial^2 \tilde{I}_1^{(r)}}{\partial \bar{\mathbf{F}} \partial \bar{\mathbf{F}}}(\bar{\mathbf{F}}) \right). \tag{88}$$

Application of the strong ellipticity condition (26) and (23) with (88) results in closed-form estimates for the onset of macroscopic instabilities in Gent composites. In particular, when the fiber and the matrix lock-up stretches are identical (i.e., $t = 1$), for the case of compression along the fibers the critical stretch ratio can be estimated from the solution of the polynomial equation

$$\begin{aligned} &\left(\bar{\lambda}_c^3 - 1\right)\left(c^{(f)}\mu^{(f)}\alpha^{(m)} + c^{(m)}\mu^{(m)}\alpha^{(f)}\right) + \bar{\mu}\alpha^{(f)}\alpha^{(m)}\left)\left(1 - 2\bar{\lambda}_c + \bar{\lambda}_c^2\right) \\ &\quad + \left(\bar{\mu}\left(\bar{\lambda}_c^3 - 1\right) + \tilde{\mu}\right)\left(\bar{\lambda}_c^4 + 2\bar{\lambda}_c - \bar{\lambda}_c^2(J_m + 3)\right) = 0. \end{aligned} \tag{89}$$

We note that as $J_m \to \infty$ this equation is reduced to the corresponding expression for the neo-Hookean composite as given in (57).

To estimate the applicability range of (88), the domain in the seven dimensional space $(\bar{\lambda},\ \Theta,\ k,\ \mu^{(m)},\ c^{(f)},\ t,\ J_m^{(m)})$ where the derivatives of $\tilde{\omega}^{(G)}$ with respect to $\bar{\mathbf{F}}$ are small and $\tilde{\omega}^{(G)}$ can be approximated by $\tilde{\omega}^{(H)}$ needs to be identified. In a way of an example, we examine the dependence of $\tilde{\omega}^{(G)}$ and $\frac{\partial \tilde{\omega}^{(G)}}{\partial \bar{\lambda}}$ on $\bar{\lambda}$. This is demonstrated in Fig. 7 for composites with fiber volume fraction $c^{(f)} = 0.5$, shear moduli ratio $k = 100$, $\mu^{(m)} = 10^6$ Pa, $t = 1$ and loading direction $\Theta = 0$. The continuous curves correspond to $\tilde{\omega}(\bar{\lambda})$ for $J_m = 0.1,\ 1,\ 10,\ 100$ and the dashed curves to the corresponding derivatives. The thin short-dash line corresponds to $\tilde{\omega}^{(H)}$ (which is independent of $\bar{\lambda}$). We observe two regions of the functions $\tilde{\omega}^{(G)}$ and $\frac{\partial \tilde{\omega}^{(G)}}{\partial \bar{\lambda}}$, a "fast" region and a "slow" one. The value of $\bar{\lambda}_s$ that separates these two regions is given by the solution of the equation

$$\tilde{\omega}^{(G)}(\bar{\lambda}_s) - \frac{\partial \tilde{\omega}^{(G)}}{\partial \bar{\lambda}}(\bar{\lambda}_s) = 0. \tag{90}$$

In Fig. 7, the curve crossings that represent the solution of (90) are marked by squares. We observe that as long as $\bar{\lambda} > \bar{\lambda}_s$, that is in the "slow" region of the two functions, $\tilde{\omega}^{(G)}$

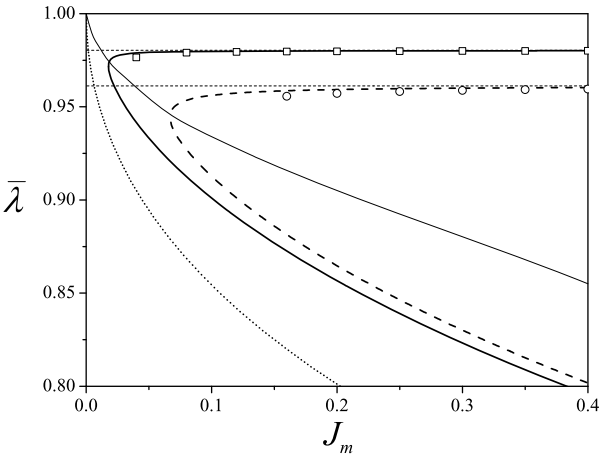

Fig. 8 The dependence of the critical stretch ratio $\bar{\lambda}_c$ on the locking parameter J_m. The *solid line* corresponds to shear moduli ratio $k = 100$, and the *dashed curve* to $k = 50$. The *dotted curve* represents the lock-up stretch ratio. The numerical simulation results are marked by *squares* and *circles* for $k = 100$ and 50, respectively

is almost identical to $\tilde{\omega}^{(H)}$. In the scale of this plot the critical stretch ratios for the four composites examined are very close and hence are marked by a single triangle mark. Since $\bar{\lambda}_c > \bar{\lambda}_s$, in these composites the ellipticity loss occurs before the $\bar{\lambda}_s$ is achieved. Even in the case when $\bar{\lambda}_c < \bar{\lambda}_s$ the upper estimate is still usable, but the difference in the predicted solution becomes large.

The results obtained by application of the upper estimate (89) for the critical stretch ratio are shown in Fig. 8 for the case of aligned compression ($\Theta = 0$). The solid curve corresponds to shear moduli ratio $k = 100$, and the dashed curve to $k = 50$. We emphasize that for the results shown in Fig. 8, the curves determined via the full solution of the variational estimate (that is with $\tilde{\omega}^{(G)}$ and its derivatives) lay on top of those determined via the upper estimate (89). The dotted curve describes the solution of the lock-up equation due to loading in the form of (61)

$$\bar{\lambda}_{lock} = \frac{1}{2}\left(\sqrt{J_m + 4} - \sqrt{J_m}\right). \tag{91}$$

The thin dashed lines are the corresponding estimates for the neo-Hookean composites. The results of the numerical simulations are also shown in Fig. 8. The square and circle marks correspond to simulations with $k = 100$ and 50, respectively. The numerical results are in good agreement with the analytical ones even in the region where the locking effect becomes significant. In a manner similar to one mentioned in connection with the neo-Hookean composites, the differences between the analytical and the numerical results are due to the effect of compressibility in the simulations and the different microstructures.

We note that in the region where the locking effect becomes significant, both phases markedly stiffens and hence the contrast between their stiffnesses decreases. Consequently, for small enough locking parameter of the Gent phases no instabilities are detected. Specifically, as can be deduced for the two families of Gent composites shown in Fig. 8, composites with $k = 100$ and $J_m < 0.018$ are stable, as well as composites with $k = 50$ and $J_m < 0.067$. We denote the minimal value of the locking parameter beneath which the composite is stable $J_m^{(c)}$. This value depends on the phases properties but particularly on k. The critical stretch ratios corresponding to $J_m^{(c)}$ are represented in Fig. 8 by a thin continuous curve.

In case when the matrix is characterized by a locking parameter smaller than that of the fiber phase (e.g., $t < 1$), the matrix stiffens faster than the fiber and the contrast between the phases decreases with the deformation. In this case the composite becomes more stable in a

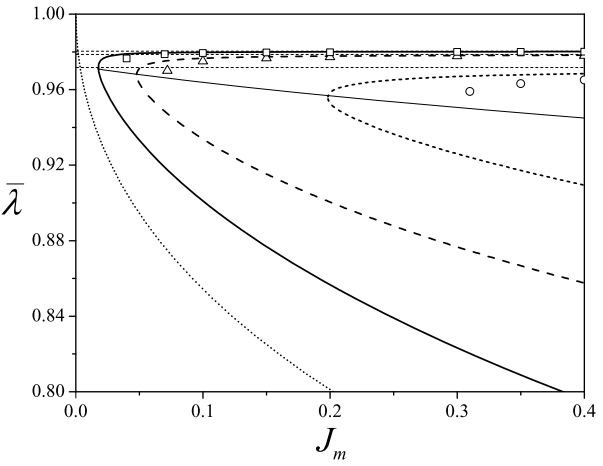

Fig. 9 The dependence of the critical stretch ratio $\bar{\lambda}_c$ on the locking parameter J_m for $k = 100$. The *solid*, *dashed* and *short-dashed curves* correspond to $\Theta = 0$, $\pi/16$ and $\pi/8$, respectively. The results of the numerical simulations are marked by *squares*, *triangles* and *circles* for $\Theta = 0$, $\pi/16$ and $\pi/8$, respectively. The corresponding solutions for the neo-Hookean composites are marked by *dashed thin lines*. The *locking curve* is the *dotted* one. The *thin continuous curve* represents the maximal loading angle for which instabilities were detected

manner similar to the case $t = 1$. The situation changes when the fiber phase stiffens faster than the matrix phase (e.g., $t > 1$). In this case, the contrast between the phases responses increases with the deformation, and the composite becomes more sensitive to compression. This finding is consistent with corresponding findings of Agoras et al. [2] that were determined via the LC variational method.

Finally, the influence of the loading direction is demonstrated for composites with $c^{(f)} = 0.5$ and $k = 100$ in Fig. 9. Shown is the dependence of the critical stretch ratio $\bar{\lambda}_c$ on the locking parameter J_m. The solid curve corresponds to aligned compression ($\Theta = 0$), the dashed and short-dashed curves represent non-aligned compression with $\Theta = \pi/16$ and $\pi/8$ respectively. The results of the numerical simulations are marked by squares, triangles and circles for $\Theta = 0$, $\pi/16$ and $\pi/8$, respectively. The corresponding solutions for the neo-Hookean composites are marked by thin dashed curves. The dotted curve describes the lock-up stretch ratios according to (91).

The difference between the numerical simulations and the analytical predictions is due to the compressibility and microstructure differences. In a manner similar to the one observed for the neo-Hookean composites, an increase of the loading angle requires a decrease of the stretch ratio to achieve the onset of a failure. Additionally, for a given locking parameter J_m there exists a loading angle $\Theta^{(c)}$ beyond which the composite becomes stable. The curve corresponding to this loading angle, which terminates at $J_m^{(c)}$ when $\Theta = 0$, is presented in Fig. 9 by the thin continuous curve.

We conclude this section noting that in both cases of aligned loading (Fig. 8) and non-aligned loading (Fig. 9), the onset of failures in the Gent composites can be conservatively estimated by the corresponding predictions for the neo-Hookean composites even for relatively small values of J_m. The proximity between the estimates for the critical stretches is in agreement with corresponding results computed by Bertoldi and Boyce [4] and Agoras et al. [2]. Bertoldi and Boyce [4] noted that for $J_m > 1$ the numerical estimates for both microscopic and macroscopic critical stretch ratios at the onset of ellipticity loss in porous composites with Gent and neo-Hookean matrices are almost identical when their microstructures are identical. Based on estimates computed for specific composites with neo-Hookean and Gent phases, Agoras et al. [2] infer that macroscopic instabilities may develop in non-linear incompressible fiber composites whenever $\bar{\lambda}_n$ reaches the critical value predicted by (57) that was derived from the TIH model of deBotton et al. [12]. Specifically, it was proposed that the estimates for the effective isochoric and out-of-plane shear moduli of the

non-linear composite in the reference configuration will be substituted for $\bar{\mu}$ and $\tilde{\mu}$ in (57), respectively.

A fundamental reasoning for the proximity of the various estimates computed for composites with identical microstructures and different behaviors of the phases was given in deBotton and Shmuel [11]. These investigators noted that the structure of the variational estimate (34) hints at the fact that bifurcations exhibited by the composite should be related to corresponding bifurcations of the associated comparison composite. This is because the corrector term depends only on the properties of the phases, and hence bifurcations cannot be associated with this term. Accordingly, whenever a secondary solution that is associated with a lower energy state branches out from the primary solution, corresponding secondary solution will branch out from the primary solution for the comparison composite as well. While the precise configurations at which the bifurcations occur in the composite and the comparison composite do not have to be identical, if the corrector terms are small the two states should be quite close. We further note that the proximity of the critical stretch ratios at the onset of instability in the two composites is not limited to the vicinity of the reference configuration (as concluded by Agoras et al. [2]). In fact, with an appropriate optimization over the properties of the comparison composite, estimates for instabilities that occur at large stretch ratios can be deduced from instability analysis of the comparison composite. Moreover, while estimate (35) that was used throughout this work was obtained by making use of a comparison composite with neo-Hookean phases, the general variational estimate (34) allows to make use of comparison composites with other types of phases. Usage of available estimates for composites with two-terms Yeoh [42] model (e.g., Shmuel and deBotton [39]) or anisotropic phases (e.g., deBotton and Shmuel [10], Lopez-Pamies and Idiart [23]) will improve the resulting estimates for critical stretch ratios away from the reference configuration.

We finally note that the proximity of the critical loading states is anticipated for the critical stretch ratios since in (34) the macroscopic deformation gradient $\bar{\mathbf{F}}$ appears in the expressions for the energy-density functions of both the composite $\hat{\Psi}$ and the comparison composite $\hat{\Psi}_0$. The same cannot be inferred for the corresponding critical stresses at the onset of ellipticity loss in the two composites since the slopes of $\hat{\Psi}$ and $\hat{\Psi}_0$ may differ quite a bit. This observation explains why Agoras et al. [2] found that while the estimates they computed for the critical stretch ratios of the neo-Hookean and the Gent composites are in good agreement, the same cannot be said for the corresponding estimates computed for the critical stresses.

6 Conclusions

This study examined both analytically and numerically the instability phenomenon in hyperelastic fiber composites. The study focused on predictions of the onset of failure due to loss of ellipticity of the governing equations describing the homogenized behavior of the composites. The analytical model involved a TI composite in which aligned stiffer fibers in a softer matrix are randomly distributed in the transverse plane. The *nonlinear-comparison* variational method of deBotton and Shmuel [11] was utilized to estimate the composites effective response. In particular, we examined composites with neo-Hookean and Gent phases. Additionally, a new upper estimate for Gent composites was introduced. In parallel, we developed a 3-D FE model and extended techniques for numerically determining the onset of ellipticity loss.

The analytical models resulted in closed-form estimates for the critical stretch ratio corresponding to the onset of failure. The critical stretch ratio depends mainly on the volume

fraction of the fiber and the contrast between the moduli of the fiber and the matrix. The higher the contrast, the less compressive strain is needed for the appearance of instabilities. The influence of the fiber volume fraction is weak for the common range of fiber volume fraction $0.2 < c^{(f)} < 0.5$ but becomes significant in the limits of low and high volume fractions.

In accordance with the analytical findings, the numerical simulations yielded different results for laminate and fiber composites. It was shown that the layered composites are more sensitive to compression than the fiber composites. Additionally, in contrast to the layered materials, the fiber composites are more stable in the range of high fiber volume fractions than at low one. For non-aligned compression we find that above a certain loading angle no instability occurs. We demonstrate that this loading angle corresponds to the state when the angle between the fiber and the load in the *deformed configuration* is $\pi/4$. At this angle the loading on the fibers switches from compression to tension.

In the limit of small locking parameter the Gent composites become stable. This is due to the stiffening of both the fiber and the matrix phases resulting in a decrease of the contrast between the instantaneous moduli. Consequently, the critical stretch ratio decreases towards the stretch ratio at which the material locks up and practically no instability occurs. At larger values of the locking parameter we find that the onset of failure of the Gent composites can be quite satisfactory predicted by the corresponding estimate for neo-Hookean composites. This finding, which is in agreement with corresponding results of Bertoldi and Boyce [4] and Agoras et al. [2], is explained in the light of the nonlinear comparison variational estimate of deBotton and Shmuel [11].

Acknowledgement This work was supported by the Israel Science Foundation founded by the Israel Academy of Sciences and Humanities (grant 1182/07).

Appendix: Kinematic Tensors of the Physically Motivated TI Invariants

The explicit expressions for the kinematic tensors of the physically motivated invariants are

$$\frac{\partial \lambda_n^2}{\partial \mathbf{F}} = 2\mathbf{F}\hat{\mathbf{L}} \otimes \hat{\mathbf{L}}, \tag{92}$$

$$\frac{\partial \lambda_p^2}{\partial \mathbf{F}} = \lambda_p^2 \mathbf{F}^{-T} - \frac{\lambda_p^2}{\lambda_n^2}\mathbf{F}\hat{\mathbf{L}} \otimes \hat{\mathbf{L}}, \tag{93}$$

$$\frac{\partial \gamma_n^2}{\partial \mathbf{F}} = \frac{2}{\lambda_n^2}(\mathbf{F}\hat{\mathbf{L}} \otimes \mathbf{C}\hat{\mathbf{L}} + \mathbf{F}\mathbf{C}\hat{\mathbf{L}} \otimes \hat{\mathbf{L}}) - 2\left(\frac{\gamma_n^2}{\lambda_n^2} + 2\right)\mathbf{F}\hat{\mathbf{L}} \otimes \hat{\mathbf{L}} \tag{94}$$

and

$$\frac{\partial \gamma_p^2}{\partial \mathbf{F}} = 2\mathbf{F} - 2\lambda_p^2 \mathbf{F}^{-T} + 2\left(\frac{\gamma_n^2 + \lambda_p^2}{\lambda_n^2} + 1\right)\mathbf{F}\hat{\mathbf{L}} \otimes \hat{\mathbf{L}} - \frac{2}{\lambda_n^2}(\mathbf{F}\hat{\mathbf{L}} \otimes \mathbf{C}\hat{\mathbf{L}} + \mathbf{F}\mathbf{C}\hat{\mathbf{L}} \otimes \hat{\mathbf{L}}). \tag{95}$$

References

1. Agoras, M., Lopez-Pamies, O., Castañeda, P.P.: A general hyperelastic model for incompressible fiber-reinforced elastomers. J. Mech. Phys. Solids **57**, 268–286 (2009)

2. Agoras, M., Lopez-Pamies, O., Ponte Castañeda, P.: Onset of macroscopic instabilities in fiber-reinforced elastomers at finite strain. J. Mech. Phys. Solids **57**, 1828–1850 (2009)
3. Aravas, N., Cheng, C., Ponte Castañeda, P.: Steady-state creep of fiber-reinforced composites: constitutive equations and computational issues. Int. J. Solids Struct. **32**, 2219–2244 (1995)
4. Bertoldi, K., Boyce, M.C.: Wave propagation and instabilities in monolithic and periodically structured elastomeric materials undergoing large deformations. Phys. Rev. B **78**, 184107 (2008)
5. Biot, M.A.: Mechanics of Incremental Deformations. Wiley, New York (1965), New-York
6. Budiansky, B.: Micromechanics. Comput. Struct. **16**, 3–12 (1983)
7. deBotton, G.: Transversely isotropic sequentially laminated composites in finite elasticity. J. Mech. Phys. Solids **53**, 1334–1361 (2005)
8. deBotton, G., Hariton, I.: Out-of-plane shear deformation of a neo-Hookean fiber composite. Phys. Lett. A **354**, 156–160 (2006)
9. deBotton, G., Schulgasser, K.: Bifurcation of orthotropic solids. J. Appl. Mech. Trans. ASME **63**, 317–320 (1996)
10. deBotton, G., Shmuel, G.: Mechanics of composites with two families of finitely extensible fibers undergoing large deformations. J. Mech. Phys. Solids **57**, 1165–1181 (2009)
11. deBotton, G., Shmuel, G.: A new variational estimate for the effective response of hyperelastic composites. J. Mech. Phys. Solids **58**, 466–483 (2010)
12. deBotton, G., Hariton, I., Socolsky, E.A.: Neo-Hookean fiber-reinforced composites in finite elasticity. J. Mech. Phys. Solids **54**, 533–559 (2006)
13. Ericksen, J.L., Rivlin, R.S.: Large elastic deformations of homogeneous anisotropic materials. Arch. Ration. Mech. Anal. **3**, 281–301 (1954)
14. Fleck, N.: Compressive failure of fiber composites. Adv. Appl. Mech. **33**, 43–117 (1997)
15. Gent, A.N.: A new constitutive relation for rubber. Rubber Chem. Technol. **69**, 59–61 (1996)
16. Geymonat, G., Müller, S., Triantafyllidis, N.: Homogenization of nonlinearly elastic materials, microscopic bifurcation and macroscopic loss of rank-one convexity. Arch. Ration. Mech. Anal. **122**, 231–290 (1993)
17. He, Q.C., Le Quang, H., Feng, Z.Q.: Exact results for the homogenization of elastic fiber-reinforced solids at finite strain. J. Elast. **83**, 153–177 (2006)
18. Hill, R.: On constitutive macro-variables for heterogeneous solids at finite strain. Proc. R. Soc. Lond. A **326**, 131–147 (1972)
19. Hill, R., Hutchinson, J.W.: Bifurcation phenomena in the plane tension test. J. Mech. Phys. Solids **23**, 239–264 (1975)
20. Horgan, C., Saccomandi, G.: A molecular-statistical basis for the gent constitutive model of rubber elasticity. J. Elast. **68**, 167–176 (2002)
21. Khisaeva, Z., Ostoja-Starzewski, M.: On the size of RVE in finite elasticity of random composites. J. Elast. **85**, 153–173 (2006)
22. Kittel, C.: Introduction to Solid State Physics, 8th edn. Wiley, New York (2004)
23. Lopez-Pamies, O., Idiart, M.: Fiber-reinforced hyperelastic solids: a realizable homogenization constitutive theory. J. Eng. Math. **68**, 57–83 (2010)
24. Lopez-Pamies, O., Ponte Castañeda, P.: Second-order estimates for the macroscopic response and loss of ellipticity in porous rubbers at large deformations. J. Elast. **76**, 247–287 (2004)
25. Lopez-Pamies, O., Ponte Castañeda, P.: On the overall behavior, microstructure evolution, and macroscopic stability in reinforced rubbers at large deformations: I—theory. J. Mech. Phys. Solids **54**, 807–830 (2006)
26. Merodio, J., Ogden, R.W.: Material instabilities in fiber-reinforced nonlinearly elastic solids under plane deformation. Arch. Mech. **54**, 525–552 (2002)
27. Merodio, J., Pence, T.J.: Kink surfaces in a directionally reinforced neo-Hookean material under plane deformation: II. Kink band stability and maximally dissipative band broadening. J. Elast. **62**(2), 145–170 (2001)
28. Michel, J.C., Lopez-Pamies, O., Castañeda, P.P., Triantafyllidis, N.: Microscopic and macroscopic instabilities in finitely strained porous elastomers. J. Mech. Phys. Solids **55**, 900–938 (2007)
29. Moraleda, J., Segurado, J., LLorca, J.: Finite deformation of incompressible fiber-reinforced elastomers: a computational micromechanics approach. J. Mech. Phys. Solids (2009), doi:10.1016/j.jmps.2009.05.007
30. Nestorovic, M.D., Triantafyllidis, N.: Onset of failure in finitely strained layered composites subjected to combined normal and shear loading. J. Mech. Phys. Solids **52**, 941–974 (2004)
31. Ogden, R.W.: On the overall moduli of non-linear elastic composite materials. J. Mech. Phys. Solids **22**, 541–553 (1974)
32. Ogden, R.W.: Non-Linear Elastic Deformations. Dover Publications, New York (1997)

33. Ogden, R.W.: Nonlinear Elasticity and Fibrous Structure in Arterial Wall Mechanics. Lecture Notes for Summer School on Modeling and Computation in Biomechanics. Graz University of Technology, Graz (2008)
34. O'Halloran, A., O'Malley, F., McHugh, P.: A review on dielectric elastomer actuators, technology, applications, and challenges. J. Appl. Phys. **104**, 071101 (2008)
35. Ponte Castañeda, P.: The effective mechanical properties of nonlinear isotropic composites. J. Mech. Phys. Solids **39**, 45–71 (1991)
36. Ponte Castañeda, P., Tiberio, E.: A second-order homogenization method in finite elasticity and applications to black-filled elastomers. J. Mech. Phys. Solids **48**, 1389–1411 (2000)
37. Qiu, G., Pence, T.: Loss of ellipticity in plane deformation of a simple directionally reinforced incompressible nonlinearly elastic solid. J. Elast. **49**, 31–63 (1997)
38. Rosen, B.W.: Mechanics of composite strengthening. In: Fibre Composite Materials, pp. 37–75. Am. Soc. Metals, Ohio (1965)
39. Shmuel, G., deBotton, G.: Out-of-plane shear of fiber composites at moderate stretch levels. J. Eng. Math. **68**, 85–97 (2010)
40. Triantafyllidis, N., Maker, B.N.: On the comparison between microscopic and macroscopic instability mechanisms in a class of fiber-reinforced composites. J. Appl. Mech., Trans. ASME **52**, 794–800 (1985)
41. Triantafyllidis, N., Nestorovic, M.D., Schraad, M.W.: Failure surfaces for finitely strained two-phase periodic solids under general in-plane loading. J. Appl. Mech., Trans. ASME **73**(3), 505–515 (2006)
42. Yeoh, O.H.: Some forms of the strain-energy function for rubber. Rubber Chem. Technol. **66**, 754–771 (1993)